The Aquatic Corrosion of International Simple Glass: Corrosion-Rate Trackers and Surface Alteration Layer Evolution at Varying Conditions

Ali Al Dabbas[1,2], Katalin Kopecskó[1*], Rachael Abu-Halimeh[2]

[1]Department of Engineering Geology and Geotechnics, Faculty of Civil Engineering, Budapest University of Technology and Economics BME, Hungary, Műegyetem rakpart 3, Budapest, Hungary,
[2]Jordan Atomic Energy Commission JAEC, Surficial Ores Processing Laboratories, Shafa Badran, Amman, Jordan

Abstract

The corrosion of the nuclear-borosilicate matrix in an anaerobic environment is delayed due to the formation of an amorphous gel layer on its glassy interface. The formation of this gel occurs at the saturation of silicic acid. In addition to the in-situ formed iron corrosion products, the metamorphic forms can also delay the gel formation, accelerating the nuclear glass corrosion. Saturated and pure water experimental models with and without Ankerite were incorporated into the standard materials characterization center (MCC) leach test for radioactive waste types at 90 °C. However, a synonymous test was allocated at 25 °C and was conducted among the reaction models. All the batch experiments on International Simple Glass (ISG)were performed at an initial pH of 6.3.

Various techniques for tracking the ISG corrosion rate have been employed and proven to be effective. As a result, the normalized weight loss of Na and Si were efficient trackers for all of the experimental systems/models; the higher the Si concentration, the lower the saturation, and vice versa. Furthermore, Na concentrations were proven to be an effective representation of the ISG corrosion rate, as they were able to produce sound ISG corrosion rate values across the experimental curing durations and circumstances when utilizing a particular conversion factor. Even at saturation, a higher reaction temperature was found to be an effective factor that enhances the ISG corrosion rate.

1. Introduction

Vitrification is considered to be the preferred method for the conditioning and immobilization of High-Level radioactive Waste (HLW) in geological formation repositories before its final disposal. Glass is stable to numerous corrosive parameters, but its durability may be affected over long periods due to essential extrinsic parameters, such as temperature, chemicals, and solvents. Vitrification entails HLW being incorporated in borosilicate glass, making it an inseparable part of the glass matrix, and eventually being discharged into stainless steel containers. Finally, non-recoverable fission products and actinides are trapped in a water-insoluble glass structure, viable for hundreds of millennia [1 – 4].

During this long storage, the direct contact with groundwater reduces the thermodynamic stability of the borosilicate glass turning it into its key elements by dissolution [5, 6]. The nuclear glass matrix behaves as standard glass would in water. Owing to the spread of water across the glass network, which is then accompanied by an ion interaction between the positive protons found in the underlying aqueous solution and alkaline metals within the glass, corrosion of the glass will occur in the saturated silica atmosphere, which sometimes contributes to the development of an amorphous gel coating on the surface; known as the Surface Alteration Layer (SAL) [7 – 10]. Hydration and interdiffusion in the glassy matrix initiate glass dissolution under static conditions. The silicate network is hydrolyzed to form a hydrated glass layer, and the glass dissolves quickly in diluted form; this is the initial phase. The hydrolysis rate slows as the solution becomes silica saturated and a passivating gel forms. Then, secondary phases develop on their surface, slowing the glass alteration rate to a new phase called the residual rate [11 – 14].

The gel is a porous silica-rich hydrated surface layer, generated by the precipitation of silica after it dissolves from the glass network [15 – 17]. The theory behind the gel layer being a glass protection layer is: that it tends to restrict diffusion exchanges between the glass surface and the surrounding aqueous solution, which prevents a thermodynamic equilibrium between the hydrated glass and the bulk solution from being achieved [18].

Ankerite is a complex carbonate mineral ($Ca(Fe, Mg, Mn)(CO_3)_2$), it is either a sedimentary iron corrosion product or a naturally metamorphosed material by-product from the corrosion of the waste steel and heaped HLW containers [19, 20]. Iron-bearing minerals in the repository platform may decelerate silicate saturation, maintain the process of glass dissolution, and affect the formation of several phases containing iron [21]. Iron minerals adversely affect the

amount of saturation of silicates to reduce or incorporate the porosity of the gel. Therefore, many research studies found them to be prevailing parameters of the glass alteration and prioritized them [22 - 30]. However, during the hydration phase of dissolution, the rapid incorporation of iron would clog the external gel porosity to the gel/Si saturated solution and reduce the alteration rate to minimal values [26, 31, 32].

In this paper, the function of Ankerite on the borosilicate corrosion in saturated and pure-water situations has been studied intensively. Ina previously published study [33], the favorable function of Ankerite on Si sorption under saturated silica conditions has been demonstrated. The current study also investigated the corrosion rate trackers of the aquatic corrosion of ISG and the SAL evolution at varying dissolution conditions; with and without Ankerite.

2. Materials and Sample Preparation

Ankerite

This research employed an Ankerite-rich geological sample from Rudabánya, Hungary. Using a tungsten carbide electrical mortar grinder, the sample was crushed into a powder. Then after, the powder was sieved, and the fraction with a grain size of 75–125 μm was collected.

Afterward, the powder was washed with distilled water and then ethanol before being dried overnight at 105 °C. The Brunauer-Emmett-Teller BET-N_2 method was used to calculate the Specific Surface Area, $SSA_{Ankerite}$ = 225 cm^2.g^{-1}.

A prior investigation on the same material [33 - 35] used Inductively Coupled Plasma - Optical Emission Spectrometry (ICP-OES) to characterize its composition, then identified it using X-Ray Powder Diffraction and elemental analysis (XRD), Figure 1.
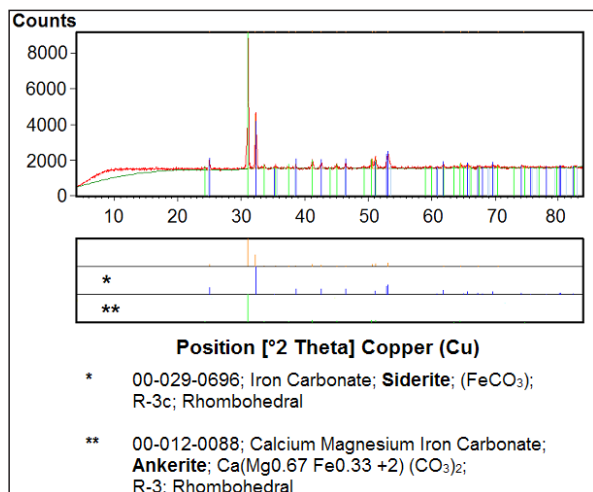

Figure 1. The XRD pattern of a natural Ankerite sample, collected from the mining area in Rudabánya, Hungary [35]

ISG

ISG is often used for testing the durability of HLW glass [36 – 41]. The ISG is a simple glass derived from its composition that aims to be an international standard. It is 6-oxide borosilicate glass with the same elemental ratios as SON68 (an inactive French R7T7 glass reference), and it is widely employed in nuclear research [1].

A 5-inch diamond saw blade was used to cut the ISG

ingot into 10*10*2 mm plates (coupons). An oil-based diamond suspension spray and polishing equipment were used to polish each ISG coupon. The Surface Area of each coupon was measured geometrically (SA=3.1cm^2), and the BET-N_2 technique was used to determine the additional surface roughness factor of 1.5.

The ISG powder was made by crushing raw ISG monoliths using a tungsten carbide ball mill device, and then sieving and collecting the fraction with a grain size < 45 μm. The powder was cleaned of fine aerosol particles by being soaked in ethanol via vacuum-driven filtration at 0.45 μm and then dried overnight at 100 °C. Equation (1) [26] was used to compute SSA_{ISG}=2,467 cm^2.g^{-1} geometrically.

$$SSA_{ISG} = \frac{\rho}{3R} \quad \text{.. (1)}$$

where; ρ is the density in g.m^{-3} (= 2.500 g.cm^{-3}) and R=10.4 μm is the average radius of a particle, which was determined by a CILAS 1190 LD Particle Size Analyser.

For this initiative, ISG samples were provided by the Savannah River National Laboratory (SRNL) in the United States. The molecular and mass oxides that make up this inactive analog glass are provided in a previous study, Table (1) [35].

Table 1. Common oxide ratios of ISG [35]

Method	Oxide	Mass (%)
ICP-OES	SiO_2	55. 6 ± 5.6
	B_2O_3	16.0 ± 1.6
	Na_2O	13.2 ± 5.1
	Al_2O_3	5.50 ± 1.1
	CaO	5.53 ± 0.6
	ZrO_2	2.98 ± 0.2
ICP-MS	Impurities	~ 0.79 ±0.1
TOTAL (%)		~ 99.6 ± 7.8

3. Methodology

The standard Materials Characterization Center (MCC) leach test for nuclear waste is one of the most regularly used static leach tests [42]. To simulate the saturated and pure-water systems, low and high Surface area to Volume ratios (S/V_{Coupon}=0.13 cm^{-1} and S/V_{Powder}=20.55 cm^{-1}) were considered by applying the MCC-1 and MCC-3 tests, respectively [7].

Polytetrafluoroethylene (PTFE) containers with a capacity of 30 mL were placed as seven (7) groups in a drying chamber for 3 days, 7 days, 14 days, 28 days, 90 days, 180 days, and 270 days to react. A temperature of 90±2 °C was chosen to expedite the reaction. After adding the ISG and Ankerite to the containers, 24 mL of ASTM Type-I water (with conductivity and resistivity of 0.055 μS.cm^{-1} 18.2 MΩ.cm, respectively) was added. All experimental containers were sealed under argon (Purity = 99.999 %) atmosphere to prevent oxidation reactions, and by adding 10 μL of 0.08 (g.L^{-1}) NaOH, the pH was adjusted to 6.3±0.2.

For each ISG+Ankerite experiment the reference trials: (i) with only ISG and (ii) with only Ankerite, were considered. The heated samples were cooled to ambient temperature after the required leaching time, and all samples were centrifuged

for 10 minutes at 4,500 rpm. At 25 °C, the pH of the leaching solution was determined immediately for all samples. After filtering the leaching solution using a Millipore filter (0.45 m pore size), 15 milliliters of the filtrate were collected for Inductively Coupled Plasma Mass Spectrometry (ICP-MS) analysis. A special abbreviation has been designed for each trial, according to Table (2).

Table 2. Abbreviations of various trials

Abbreviation	Description
RGC90	Reference Glass Coupon, reaction at 90 °C
RGP90	Reference Glass Powder, reaction at 90 °C
RAP90	Reference Ankerite Powder, reaction at 90 °C
GC90	Ankerite + Glass Coupon, reaction at 90 °C
GP90	Ankerite + Glass Powder, reaction at 90 °C
RGP25	Reference Glass Powder, reaction at 25 °C
RAP25	Reference Ankerite Powder, reaction at 25 °C
GP25	Ankerite + Glass Powder, reaction at 25 °C

By subtracting the identical element concentrations in the reference RAP, the correct element concentrations in the (Ankerite+ Glass) systems were calculated.

4. Results

4.1 Weight Loss (WL) Calculations

To achieve sound readings, the weight loss tests were performed at room temperature. Figure (2) displays the coupons, which reacted in presence of Ankerite, after leaching and provides a bar diagram showing the percentage reduction of weight. The powdered ISG samples developed higher weight loss values than the ISG coupon samples as a consequence of the higher interdiffusion due to their higher S/V ratios. Also, the dissolved silica was shown to re-precipitate on the ISG coupon surface and be incorporated into an amorphous gel layer, contributing to the final mass of the coupon and concluding in a lower recorded WL value. Consequently, weight loss estimates do not reflect the glass corrosion's definite value at the early stages of leaching [7]. In contrast, these measurements are of particular significance when conducting glass dissolution experiments.

Regarding the GC90 system, containing Ankerite, Figure (2) shows that on day 3 the weight loss was at its minimum value, it then continued to double to reach its maximum value on day 270; signaling that the Ankerite incorporation into the SAL decreases gradually over time while the coating layer becomes crystallized in nano-scale [43]. The (evolution/dissolution) mechanism [44, 45] on the alteration layer poses an additional reason for removing the adhered Ankerite, recalling that even when the coupons were washed with ASTM Type-I water for 10 seconds and then dried in the vacuum oven at 50 °C for 24 hours, the red color of the altered coupons is more obvious at low reaction times, as observed in Figure (2).

The ISG reference samples, however, initially exhibited unfavorable behavior, and the loss value reached a maximum, during the first month of reaction, on day 14. It then declined and remained constant. As mentioned earlier, during glass corrosion, many separate steps occur, including reactions, diffusion, and precipitation. During the reaction, the rate

determination phase can vary and rely heavily on the test parameters.

The WL analysis provided sufficient primary insight into the ISG corrosion rates. In comparison to Figure (3) later in this article, the WL per unit area of the glass interface might be regarded as an acceptable indication, capable of yielding the same forecast on the subsequent analysis. However, since tracking the boron (B) concentrations in the typical technique for measuring the precise corrosion rate, this method is insufficient. One observation derived from Figure (2) is that the SAL transforms over time from a foam/colloidal structure to a crystal form, this prevents the Ankerite from cohering to the SAL surface.
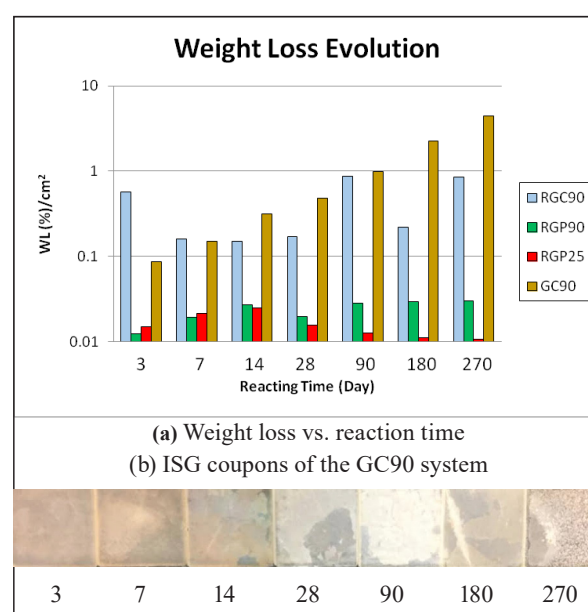

(a) Weight loss vs. reaction time
(b) ISG coupons of the GC90 system

Figure 2. The weight loss per unit area of altered ISG in all systems and the evidence of the formation of amorphous silica in the first hours of a reaction by showing the Ankerite cohering on the SAL of ISG coupon. (a) Chart showing the ISG-weight loss percentage per unit surface area as an indication of the ISG corrosion (b) ISG coupons of the GC90 system after curing. Over time, Ankerite was detaching with (evolution/dissolution) of the SAL

4.2 ISG Corrosion Tracers

The Normalized weight Loss () was calculated using Equation (2) [7] for the main elements resulting from the dissolution of the glass samples (Na, B, Si, Ca, Al); concentrations of Zr were not sufficient for such calculations.

$$NL_i = \frac{m_i}{f_i.SA} \quad \text{...} (2)$$

where; : the mass of element i in the leachate, f_i: mass fraction of element i in the unleached solid (unitless), and SA: sample geometric Surface Area (m²).

Boron is commonly used to monitor glass corrosion rates (CR$_{ISG}$) [7, 46]. Figure (3) shows the corrosion rates for all the experimental systems. The correct boron concentrations were determined in the ISG-Ankerite (GC90, GP90, and GP25) systems by excluding the apparent boron concentrations in the reference (Ankerite-water) systems (RAP90, RAP25) with taking into account the surface area to volume value in each vessel. The ISG corrosion rate in Figure (3)was calculated by applying the following Equations (3 and 4), which were used by Neill et al. [29] for ISG:

$$CR_{ISG} = \frac{d(E_{th(B)})}{dt} \quad \text{...............................} \quad (3)$$

where; CR_{ISG} is ISG corrosion rate (nm.d^{-1}) and is the equivalent thickness (altered ISG) of Boron (nm) that can be calculated from the following relation:

$$E_{th(i)} = \frac{NL_i}{\rho_{ISG}} \quad \text{.......................................} \quad (4)$$

where: is the density of ISG (2.5 g.cm^{-3}).
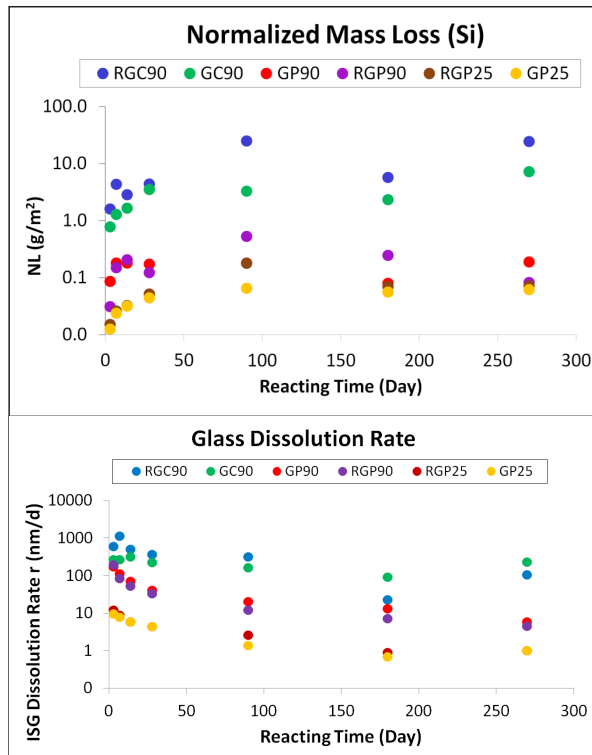
Normalized Mass Loss (Si)

Figure 3. Silicon normalized loss NL_{Si} and ISG dissolution rate CR_{ISG} in all systems

It is apparent that the temperature and S/V ratio have opposite effects on both the NL_{Si} and CR_{ISG}; this is seen to be indirect with S/V, although the presence of Ankerite slightly lowered their values in GC90 and the contrary occurred in GP90. The NL_{Si} increased with time, but the CR_{ISG} was found to decrease with time. (Each point = single experiment)

4.2.1 Silicon Concentrations

In the saturated system, the silicon normalized weight loss (NL_{Si}) values have been seen as the dominant factor of CR_{ISG}, as described in Figure (3). Compared to the ISG-coupon (pure-water) systems, the ISG-powdered (saturated) systems generated significantly lower NL_{Si} results. This implies that once the concentration of soluble silica species in the aqueous phase reaches saturation, no more glass dissolution would occur, and the saturation of amorphous silica may not represent the thermodynamic saturation of the glass network. [15]. The analysis also revealed that the S/V effect is significantly greater than the effect of other parameters (i.e., temperature); however, the NL_{Si} results revealed that the GP90 model was up to ten (10) orders more effective than the GP25 model. It is worth mentioning that Ankerite reference tests have been prepared and leached in the same conditions: pH, time, and temperature for both the ISG/Ankerite and the water systems. The findings of the blank sample were used to promote the calculation of NL_{Si} only arising from ISG corrosion.

The inversely proportional relationship seen in Figure (3)

between the period of leaching and the CR_{ISG} may be due to normalized weight transmission through layers formed as glass corrodes or increased concentrations of glass corrosion in the solution. This reduces the driving force of mass transfer, which slows down each reaction that releases these components. In this context, except for Si, the overall normalized weight loss of the main ISG corrosion products (B, Ca, Al, Na) are attached in the Appendix.

The involvement of Ankerite in the ISG coupon 90 °C (GC90) and the ISG powder 25 °C (GP25) systems has lowered the (NL_{Si}) and (CR_{ISG}) values up to 90 days of reaction; the opposite occurred, however, from day 180 of reaction. On day 7 of the reaction, the GP90 glass powder system was the same, suggesting that the higher S/V was forecast to increase the Ankerite impact on ISG dissolution. The previous results show that the rapid precipitation of silicate compounds can cause an increase in ISG dissolution at higher S/V and temperature values with Ankerite presence. However, the concentrations of Ca in ISG powder systems RGP90, and GP90 were below the detection limit (BDL) during the reaction cycle, which may mean that Ca was preferably retained at higher S/V and temperature (Appendix) instead of Na [47], or that gel porosity was possibly clogged [48]. Boron levels have been constantly demonstrated to be higher than silicon levels (Figure 3) typically related to the dissolution of borosilicate glass [7].

In presence of sorptive compounds (i.e., iron corrosion products which are represented in this research by Ankerite) silicon concentrations are generally not consistent with ISG corrosion's behavior due to silica sorption reactions and possible precipitation [7]. This may be justified by Si precipitation (i.e., Mg-Si); nevertheless, it is worth mentioning here that in prior research, Ankerite has been shown to initiate late (at day 90) Mg-Si precipitation and early Si sorption.[33, 35].

4.2.2 Sodium Concentrations

The current experiment has also been used to assess if sodium for the given corrosion stage may be regarded as a tracer factor for the rate of glass corrosion. In Figure (4) extracted from Table (3), the average CR_{ISG} contribution for the whole experiment is summarized and the effect of Ankerite on various systems can be noticed. In particular, Ankerite raised the CR_{ISG} to higher values in the ISG coupon system (i.e., on days 180, and 270). But the overall CR_{ISG} average over the whole treatment period was different. Both stress the above-mentioned assumption about sodium. Therefore, these observations can be stated:

In terms of behavior, the values of NL_{Na} and CR_{ISG} were equivalent.

In ISG powder systems, Ankerite did not affect the CR_{ISG}. (That is, the average value of RGP90 and GP90, as well as the average value of RGP25 and GP25, were nearly identical).

Regardless of the presence of Ankerite, the CR_{ISG} average of the ISG powdered systems at 25 °C was the lowest of all systems, while the CR_{ISG} of the 90 °C powders was higher by 10 orders.

At 90 °C, the CR_{ISG} averages of the ISG coupon systems were the highest of all systems. In addition, the CR_{ISG} was decreased by 10 orders when moving from RGP90 to RGC90 and was decreased by 5 orders when moving from GP90 to GC90.

As a result of the above observation, Ankerite cut the CR_{ISG} in ISG coupon systems in half. (i.e., CR_{ISG} in RGC90 equals 2*CR_{ISG} in GC90).

Table 3. Average normalized loss and average glass corrosion rates at day 270

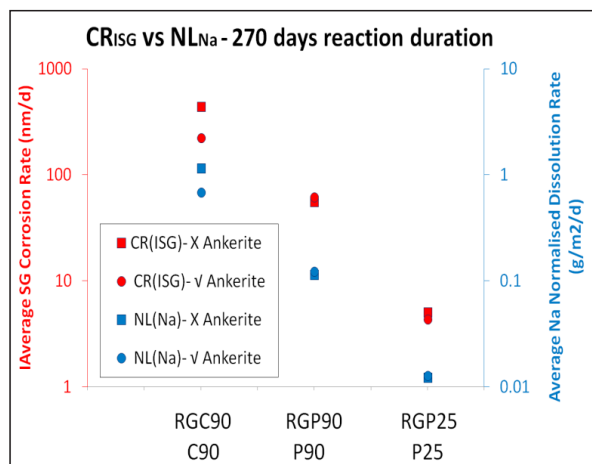| System	Ankerite Presence	NL_{Na} (g.m⁻².d⁻¹)	CR_{ISG} (nm.d⁻¹)
RGC90	-	1.154 ± 0.192	440.5 ± 17.6
RGP90	-	0.114 ± 0.020	55.98 ± 2.34
RGP25	-	0.012 ± 0.002	5.090 ± 0.22
GC90	Yes	0.686 ± 0.118	224.3 ± 8.96
GP90	Yes	0.123 ± 0.021	62.10 ± 2.58
GP25	Yes	0.013 ± 0.003	4.368 ± 0.215

Figure 4. Average Na normalized loss VS Average Glass.
Corrosion Rates at day 270 for all categories. (Each point = average of 7 experiments)

In this regard, Ebert[7] mentioned that "normalized mass losses of sodium and the pH values at different S/V values show that tests at lower S/V values attain higher sodium releases and higher corrosion rates based on sodium release. Tests at higher S/V generate solutions with higher pH values and higher sodium concentrations but lower glass corrosion rates when expressed as mass glass dissolved per unit area". Throughout the current experiment, the listed details are evidenced by the ISG.

5. Discussion

In light of the above findings, the effect of Ankerite on the rate of glass corrosion in pure-water systems (RGC90, GC90) is significant because it affects the solution's chemistry and hence the rate of glass corrosion via chemical parameters. In comparison to the ISG reference model (RGC90), Ankerite appears to be successful in lowering the ISG corrosion rate primarily by increasing the pH [49] and also by clogging the initial rate [34]. That was true for all corrosion rate observations between days 3 and 90, given that the aforementioned assumption is violated when the system approaches saturation with amorphous silica.

Meanwhile, Ankerite enhanced the corrosion rate

slightly more than its reference RGP system in saturated systems, which may be due to the aggressive consumption effect on Si via sorption and precipitation with Fe and Mg [33, 34, 35].

In this paper, the words silica and silica saturation are not used to refer to dissolved SiO_2. In contrast, the more dissolved SiO_2 means more glass corrosion as well as more accumulated silicic acid in the forward stage, this is demonstrated while comparing the evolution of Si with B normalized losses.

Dissolution/precipitation responses were observed between Si and the soluble elements by the diffusion of Ankerite components. That is stressed by Delage et al. and Grambow [50, 51] that glass dissolution is regulated by orthosilicic/silicic acid action in solution in their static leaching studies on French R7T7 non-radioactive reference borosilicate glass in distilled water at 90 °C. Owing to the higher S/V ratio in the powdered ISG experiments, Si concentrations were far higher than in glass coupon systems. However, this work's short time scale limited the requirements, as in ISG coupon systems, silicic acid (H_4SiO_4) saturation was not adequately achieved; however, in ISG powder systems, it was already achieved during the reaction's first hours.

The difference in ISG mass was detected, using an electrical balance, before and after leaching. An alternative method was implied to calculate the mass loss using the values obtained by ICP-MS, by finding the total mass of elements (B, Na, Al, Si, Ca, Zr) transferred to the aqueous solution. The values obtained by both methods were in good agreement and any differences can be attributed to the SAL (evolution/dissolution) weight in (mg). The mass fraction of dissolved X_g glass was represented by Neeway et al. [45], and was calculated by Equation (5).

$$X_g = \frac{NL_i \times S_g}{M_g} \quad .... (5)$$

where; NL_i is the normalized mass loss for a given period (g.m⁻²), is the surface area of the original glass (m²) and is the initial mass of the glass (g).

Equation (6) was attained by inserting the normalized loss (NL) formula Equation (2) into the X_g formula Equation (5) for calculating the overall mass fraction of ISG $X_{g(overall)}$ dissolved in solution:

$$X_{g(overall)} = \frac{m_i}{M_g} \quad .... (6)$$

Figure (5) illustrates calculated and measured weight loss values for all systems except those containing both powdered ISG and Ankerite. Equation (7) is based on the assumption that the difference between the calculated and measured ISG weights results in an estimate of the SAL's (evolution/dissolution) weight. In light of the NL_{Si} in the solution, this layer is mostly silica gel (amorphous silica SiO_2). ISG is primarily composed of the oxides listed in Table (1). At a total concentration of < 1.0 % [38], the ISG's impurities (Cr, P, K, Fe, Ni, Mn, Mg, S, Ti, F, and Cl) are defined. The existence of these impurities was incorporated in the overall uncertainty of 15 % of the estimated SAL's (evolution/

dissolution) weight as a ~ 1.0 % of the total concentration referred to as impurities.

$$W_{SAL} = WL - W_{i(overall)}$$ .... (7)

where; $W_{i(overall)}$ (mg) is the calculated weight of the dissolved elements as obtained by ICP-MS analyses, and WL (mg) is the measured loss in weight in ISG via a Mettler Toledo electrical balance.
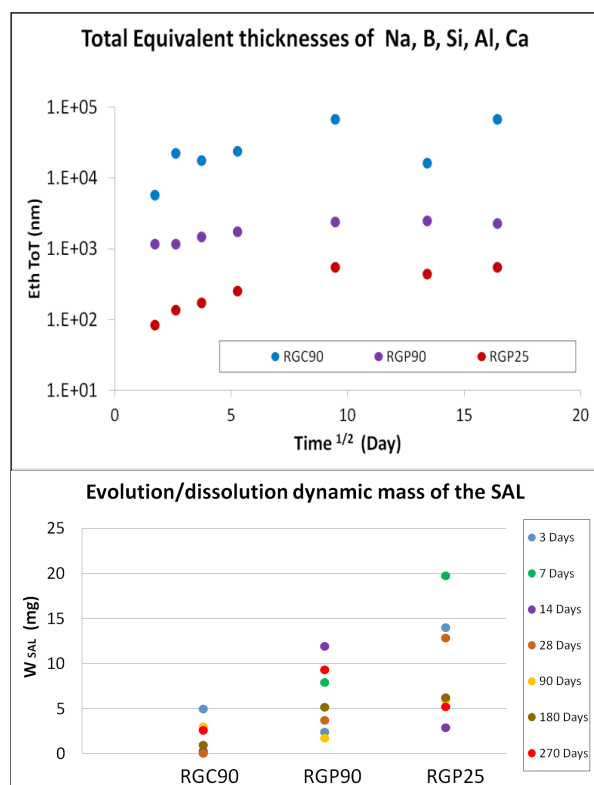

Figure 5. The total equivalent thickness of the ISG corrosion products and the estimated dynamic mass (evolution/dissolution) of the surface alteration layer over time. A ± 15 % uncertainty is considered. (Each point = single experiment).

In the reference powdered glass at 25 °C, RGP25, the maximum (evolution/dissolution) on the SAL was produced. Because of the difficulties in extracting the glass when combined with the Ankerite, it should be noted that these weight reduction measures were only performed on the comparison (reference) glass samples. The highest SAL's dynamic mass of all the systems reached approximately 20 mg in RGP25.

According to the data given, it appears as though a thick silica layer is formed at the interface of the glass coupon as a result of the cooling and drying of an interfacial solution rich in dissolved silica. This solution occurs as the thickness of the SAL develops and aqueous silica can no longer be successfully transferred away from the evaporation/ dissolution boundary to the bulk solution. As a result, silicic acid and other glass constituents accumulate at the ISG interface, resulting in aggregation and gelation. As a result, less silicic acid may be removed from the glass, transported, and dissolved into the interfacial suspension or gel, thereby decreasing the surface-controlled dissolving process and favoring interdiffusion. And this may explain and justify the varying rates of weight loss in the case of RGP90 and RGC90.

SAL's dynamic mass (W_{SAL}) differed more in the first 28 days of reaction between the RGP90 and RGC90 models. Higher S/V values appear to intensify the glass alterations during the first aging process independent of Ankerite's existence. This highlights a hypothesis described above that the Ankerite's impact in the first month of reaction should not be considered. Compared to the overall equivalent (altered ISG) thickness ($E_{th(total)}$) of the main ISG elements, which has been calculated for all ISG corrosion products by using Equation (4), the W_{SAL} values had reverse effects and RGP25 showed the highest measurements. The order of the systems concerned is reversely consistent with the order of the specimens in the field of CR_{ISG}; RGP25 < RGP90 < RGC90, which sounds logical according to to experiment observations, based on the capacity for large-scale gel for evolution/dissolution [44, 45].

6. Conclusions

Ankerite has a negligible influence on the rate of ISG corrosion during the initial stage of the reaction. This idea was reinforced by weight loss estimates, which, however, do not accurately reflect the definite value of glass corrosion.

When the concentration of soluble silica species in the aqueous phase approaches saturation; no further glass dissolution occurs. However, sodium normalized mass loss results indicated that pure-water test values result in higher sodium releases and corrosion rates based on sodium release. When stated in terms of glass mass dissolved per unit area, saturated test systems had greater sodium concentrations but lower rates of glass corrosion.

In this study, a new method was used to determine the dynamic mass of the surface alteration layer. This method showed that a high dynamic mass coincides with a low corrosion rate, resulting in low ISG components' equivalent thickness.

Compliance with ethical standards

Conflict of interest: The authors declare that they have no conflict of interest.

References

Gin S, Ryan J, Kerisit S, Du J, Simplifying a solution to a complex puzzle, npj Materials Degradation (2018). doi:10.1038/s41529-018-0057-y

ANDRA, Evaluation of the feasibility of a geological repository in an argillaceous formation, Report Series, France, Dossier, (2005).

World Nuclear Association, 2017, Treatment and conditioning of nuclear waste, World Nuclear Association, 2017

https://www.world-nuclear.org/information-library/nuclear-fuel-cycle/nuclear-wastes/treatment-and-conditioning-of-nuclear-wastes.aspx

World Nuclear Association, 2020, Radioactive Waste Management, World Nuclear Association, 2020.

https://www.world-nuclear.org/information-library/nuclear-fuel-cycle/nuclear-wastes/radioactive-waste-management.aspx

Paul, A. (1977). Chemical durability of glasses; a thermodynamic approach. Journal of Materials Science, 12(11), 2246–2268.

Jollivet P., Frugier P., Parisot G., Mestre J. P., Brackx E., Gin S., & Schumacher, S. (2012). Effect of clayey groundwater on the dissolution rate of the simulated nuclear waste glass SON68. Journal of Nuclear Materials, 420(1-3), 508–518.

https://doi.org/10.1016/j.jnucmat.2011.10.026

Ebert, W L. The effects of the glass surface area/solution volume ratio on glass corrosion: A critical review. United States: N. p., 1995. pp.18-79.doi:10.2172/67461

Bouakkaz R., Abdelouas A., El Mendili Y., Grambow B., Gin S. SON68 glass alteration under Si-rich solutions at low temperature (35–90 °C): kinetics, secondary phases, and isotopic exchange studies, RSC Adv, Vol. 6, 2016, pp. 72616–72633.

https://doi.org/10.1039/C6RA12404F

El Hajj H., Abdelouas A., Grambow B., Martin C., Dion M. Microbial corrosion of P235GH steel under geological conditions, Physics and Chemistry of the Earth, Parts A/B/C, 35 (6-8), 2010, pp. 248–253.doi:10.1016/j.pce.2010.04.007

Gin S. Open scientific questions about nuclear glass corrosion, Procedia Materials Science, Vol. 7, 2014, pp. 163–171.doi: 10.1016/j.mspro.2014.10.022

De Echave T., Tribet M., Jollivet P., Marques C., Gin S., Jégou C., (2018). Effect of clayey groundwater on the dissolution rate of SON68 simulated nuclear waste glass at 70 °C. Journal of Nuclear Materials, S002231151731142X–.

doi:10.1016/j.jnucmat.2018.03.013

Van Iseghem P., Aertsens, M., Lemmens, K., Gin S., Deneele D., Grambow B., McGrail P., Strachan D., Wicks G., McMenamin T., Glamor: A Critical Evaluation of the Dissolution Mechanisms of High-level Waste Glasses in Conditions of Relevance for Geological Disposal INIS-FR-3271; The Sixth International Conference on the Management and Disposal of Radioactive Waste, France, 2004; pp 781−785.

Van Iseghem P., Aertsens M., Gin S., Deneele D., Grambow B., Strachan D., McGrail P., G. Wicks, GLAMOR: How we Achieved a Common Understanding on the Decrease of Glass Dissolution Kinetics, in: A. Cozzi, T. Ohji (Eds.), Environmental Issues and Waste Management Technologies in the Materials and Nuclear Industries Xii, Amer Ceramic Soc, Westerville, 2009, pp. 115-1

Vienna D., Ryan V., Gin S., Inagaki Y., (2013). Current Understanding and Remaining Challenges in Modeling Long-Term Degradation of Borosilicate Nuclear Waste Glasses. International Journal of Applied Glass Science, 4(4), 283–294. doi:10.1111/ijag.12050

Frankel G. S., Vienna J. D., Lian J., Guo X., Gin S., Kim S. H., … Scully J. R. (2021). Recent Advances in Corrosion Science Applicable To Disposal of High-Level Nuclear Waste. Chemical Reviews. doi:10.1021/acs.chemrev.0c00990

Gin S., Neill L., Fournier M., Frugier P., Ducasse T., Tribet M., Abdelouas A., Parruzot B., Neeway J., Wall N., (2016). The controversial role of inter-diffusion in glass alteration. Chemical Geology, 440, 115–123. doi:10.1016/j.chemgeo.2016.07.014

Pierce M., Frugier P, Criscenti J., Kwon D., Kerisit N. (2014). Modeling Interfacial Glass-Water Reactions: Recent Advances and Current Limitations. International Journal of Applied Glass Science, 5(4), 421–435. doi:10.1111/ijag.12077

Gin S., Mestre J.P., (2001). SON 68 nuclear glass alteration kinetics between pH 7 and pH 11.5. , 295(1), 83–96. doi:10.1016/s0022-3115(01)00434-2

Chai L., Navrotsky A.. (1996), Synthesis, characterization, and energetics of solid solution along the dolomite-ankerite join, and implications for the stability of ordered CaFe(CO3)2, American Mineralogist, 81 (9-10), pp. 1141–1147.

https://doi.org/10.2138/am-1996-9-1012

Ellwood B. B., Burkart B., Rajeshwar K., Darwin R. L., Neeley R. A., McCall A. B., … Hickcox C. W. (1989), Are the iron carbonate minerals, ankerite, and ferroan dolomite, like siderite, important in paleomagnetism? Journal of Geophysical Research, 94(B6), 7321. https://doi.org/10.1029/JB094iB06p07321

Bart G., Zwicky H. U., Aerne E. T., Graber T. H., Berg D. Z, Tokiwai M. (1986), Borosilicate glass corrosion in the presence of steel corrosion products, Materials Research Society fall meeting, Boston, MA, USA, 1-5 December 1986, Vol. 18, No. 22,1986, pp. 459–470. https://inis.iaea.org/search/search.aspx?orig_q=RN:18091173

Burger E., Rebiscoul D., Bruguier F., Jublot M., Lartigue J. E., Gin S.. (2013), Impact of iron on nuclear glass alteration in geological repository conditions: A multiscale approach, Applied Geochemistry, Vol. 31, pp. 159–170.

http://dx.doi.org/10.1016/j.apgeochem.2012.12.016

Carriere C., Neff D., Foy E., Martin C., Linard Y., Michau N., Dynes J., Dillmann P.. (2017), Influence of iron corrosion on nuclear glass alteration processes: nanoscale investigations of the iron-bearing phases, Corrosion Engineering, Science and technology, vol. 52, no. S1, 166–172.

https://doi.org/10.1080/1478422X.2017.1306962

Debure M., Frugier P., Windt L. D., & Gin S.. (2013), Dolomite effect on borosilicate glass alteration. Applied Geochemistry, 33, 237-251.

doi:10.1016/j.apgeochem.2013.02.019

Dillmann P., Gin S., Neff D., Gentaz L., Rebiscoul D. (2016), Effect of natural and synthetic iron corrosion products on silicate glass alteration processes, Geochimica et Cosmochimica Acta, Vol. 172, pp. 287–305.

https://dx.doi.org/10.1016/j.gca.2015.09.033

Guo X., Gin S., Liu H., Ngo D., Luo J., Kim S. H., Frankel G. S.. (2020). Near-field corrosion interactions between glass and corrosion-resistant alloys. Npj Materials Degradation, 4(1). https://doi.org/10.1038/s41529-020-0114-1

Jordan N., Marmier N., Lomenech C., Giffaut E., Ehrhardt J. J.(2007), Sorption of silicates on goethite, hematite, and magnetite: Experiments and modeling, Journal of Colloid and Interface Science, 312 (2), pp. 224–229. doi:10.1016/j.jcis.2007.03.053

Michelin A., Burger E., Rebiscoul D., Neff D., Bruguier F., Drouet E., Dillmann P., and Gin S. (2013), Silicate Glass Alteration Enhanced by Iron: Origin and Long-Term

Implications, Environmental Science & Technology, 47 (2), 750-756.

doi: 10.1021/es304057y

Neill L., Gin S., Ducasse T., De Echave T., Fournier M., Jollivet P., WallN. A. (2017), Various effects of magnetite on international simple glass (ISG) dissolution: implications for the long-term durability of nuclear glasses. Npj Materials Degradation, 1(1).doi:10.1038/s41529-017-000

Philippini V., Naveau A., Catalette H., Leclercq S. (2006), Sorption of silicon on magnetite and other corrosion products of iron, Journal of Nuclear Materials, Vol. 348, No. 1-2, pp. 60–69. https://doi.org/10.1016/j.jnucmat.2005.09.002

Aréna H., Rébiscoul D., Podor R., Garcès E., Cabie M., Mestre J.-P., &Godon N. (2018), Impact of Fe, Mg and Ca elements on glass alteration: Interconnected processes. Geochimica et CosmochimicaActa, 239, 420–445. doi:10.1016/j.gca.2018.08.007

Jollivet P., Angeli F., Cailleteau C., Devreux F., Frugier P., Gin S. (2008). Investigation of gel porosity clogging during glass leaching, Journal of Non-Crystalline Solids, Vol. 354,No. 45-46, pp. 4952–4958. http://doi.org/10.1016/j.jnoncrysol.2008.07.023

Kopecskó K., DabbasA. A. (2021).Silicate Sorption on Ankerite from a Standard Silicate Solution. Periodica Polytechnica Chemical Engineering, 65(3).

https://doi.org/10.3311/ppch.16967

Dabbas A. A., KopecskóK. (2021). Corrosion of glass used for radioactive waste disposal influenced by Ankerite, Advanced Aspects of Engineering Research, Vol. 9, Chapter 10 - Book Publisher International.

http://dx.doi.org/10.9734/bpi/aaer/v9/1997F

Dabbas A. A., KopecskóK. (2021). Corrosion of International Simple Glass by Mg-Si Precipitation in Presence of Ankerite, Pollack Periodica.

doi:10.1556/606.2021.00410

Daniel J. Backhouse, Adam J. Fisher, James J. Neeway, Claire L. Corkhill, Neil C. Hyatt, Russell J. Hand, Corrosion of the International Simple Glass under acidic to hyperalkaline conditions, npj Materials Degradation, 2. 29 (2018).

doi:10.1038/s41529-018-0050-5

Guerette M, Huang L, In-situ Raman, and Brillouin light scattering study of the international simple glass in response to temperature and pressure, Journal of Non-Crystalline Solids 411 (2015) 101–105.

https://doi.org/10.1016/j.jnoncrysol.2014.12.028

Kaspar, T. C., Ryan, J. V., Pantano, C. G., Rice, J., Trivelpiece, C., Hyatt, N. C., Smith, N. J. (2019). Physical and optical properties of the International Simple Glass. Npj Materials Degradation, 3(1).doi:10.1038/s41529-019-0069-2

Neill, L., Gin, S., Ducasse, T., De Echave, T., Fournier, M., Jollivet, P., Wall, N. A. (2017). Various effects of magnetite on international simple glass (ISG) dissolution: implications for the long-term durability of nuclear glasses. Npj Materials Degradation, 1(1).doi:10.1038/s41529-017-000

Fournier, M., Ducasse, T., Pérez, A., Barchouchi, A., Daval, D., & Gin, S. (2019). Effect of pH on the stability of passivating gel layers formed on International Simple Glass. Journal of Nuclear Materials.doi:10.1016/j.jnucmat.2019.06.029

Inagaki Y, Kikunaga T, Idemitsu K, Arima T, Initial Dissolution Rate of the International Simple Glass as a Function of pH and Temperature Measured Using Microchannel Flow-Through Test Method, International Journal of Applied Glass Science, 4 [4] 317–327 (2013).https://doi.org/10.1111/ijag.12043

Strachan, D., Turcotte, R. P., & Barnes, B. O. (1982). MCC-

1: A Standard Leach Test for Nuclear Waste Forms. Nuclear Technology, 56(2), 306-312.

doi:10.13182/nt82-a32859

Ferrand K., Klinkenberg M., Caes S., Poonoosamy J., Van Renterghem W., Barthel J., Lemmens, K., Bosbach D., Brandt F. Dissolution Kinetics of International Simple Glass and Formation of Secondary Phases at Very High Surface Area to Solution Ratio in Young CementWater. Materials 2021, 14, 1254.

doi.org/10.3390/ma14051254

Gin S., & Frugier P. (2002). SON68 Glass Dissolution Kinetics at High Reaction Progress: Experimental Evidence of the Residual Rate. MRS Proceedings, 757.

Neeway J., Abdelouas A., Grambow B., & Schumacher S. (2011). Dissolution mechanism of the SON68 reference nuclear waste glass: New data in a dynamic system in silica saturation conditions. Journal of Nuclear Materials, 415(1), 31–37.

doi:10.1016/j.jnucmat.2011.05.027

Ebert, W. L., & Mazer, J. J. (1993). Laboratory Testing of Waste Glass Aqueous Corrosion; Effects of Experimental Parameters. MRS Proceedings, 333.

https://doi.org/10.1557/PROC-333-27

Debure, M., Frugier, P., De Windt, L., & Gin, S. (2012). Borosilicate glass alteration driven by magnesium carbonates. Journal of Nuclear Materials, 420(1-3), 347–361.

https://doi.org/10.1016/j.jnucmat.2011.09.032

Jollivet P., Angeli F., Cailleteau C., Devreux F., Frugier P., Gin S. Investigation of gel porosity clogging during glass leaching, Journal of Non-Crystalline Solids, Vol. 354,No. 45-46, 2008, pp. 4952–4958.doi:10.1016/j.jnoncrysol.2008.07.023

Dabbas AA, Kopecskó K. (2022). The Influence of the Saturation on the Rate of ISG Corrosion in Presence of Ankerite. IOP Conference Series: Materials Science and Engineering. (Paper in Press).

Delage F., Ghaleb D., Dussossoy J. L., Chevallier O., & Vernaz E. (1992). A mechanistic model for understanding nuclear waste glass dissolution. Journal of Nuclear Materials, 190, 191–197.https://doi.org/10.1016/0022-3115(92)90086-Z

Grambow, B. (1984). A General Rate Equation for Nuclear Waste Glass Corrosion. MRS Proceedings, 44.https://doi.org/10.1557/PROC-44-15

Appendix

Normalized loss in details for the primary elements (Na, B, Si, Al) in all leaching systems